Available online at www.sciencedirect.com

ScienceDirect

Physics Procedia 78 (2015) 99 – 109

Physics Procedia

15th Nordic Laser Materials Processing Conference, Nolamp 15, 25-27 August 2015, Lappeenranta, Finland

Measuring the melt flow on the laser cut front

Jetro Pocorni[a]*, Dirk Petring[b], John Powell[a], Eckard Deichsel[c], Alexander F.H. Kaplan[a]

[a]*Department of Engineering Sciences and Mathematics, Luleå University of Technology, Luleå 971 87, Sweden*
[b]*Fraunhofer ILT, Steinbachstr. 15, Aachen 52074, Germany*
[c]*Bystronic Laser AG, Industriestr. 21, Niederönz CH-3362, Switzerland*

Abstract

The flow characteristics on the laser cut front for 10mm stainless steel AISI 304 (EN 1.4301) are studied in this paper using High Speed Imaging (HSI). The laser cut samples were produced with a 6kW fiber laser with nitrogen gas assist. Previous work in this field has used unusual cutting parameters to make the experimentation easier. This work presents, for the first time, HSI results from standard commercially viable cutting parameters. This was made possible by the development of a new experimental technique. The results presented here suggest that the cut front produced when cutting stainless steel with a fiber laser and a nitrogen assist gas is covered in bumps which themselves are covered in a thin layer of liquid. Under the conditions shown here the bumps move down the cut front at an average speed of approximately 0.4m/s. The liquid flows at an average speed of approximately 1.1m/s. The average melt depth at the bottom of the cut zone under these conditions is approximately 0.17 mm.

Peer-review under responsibility of the Lappeenranta University of Technology (LUT)

Keywords: Laser cutting; fiber laser; melt flow; particle tracking velocimetry; high speed photography

1. Introduction

In laser fusion cutting of metals a volume of melt is created (by absorption of the laser beam) and then blown out of the cut zone by an inert assist gas (see Fig. 1).

* Corresponding author. Tel.: +46 (0) 722 330 554
E-mail address: Jetro.Pocorni@ltu.se

Peer-review under responsibility of the Lappeenranta University of Technology (LUT)
doi:10.1016/j.phpro.2015.11.022

I. Nomenclature

d	: Material thickness
D	: Cutting depth
Kr	: Kerf removal rate
Lr	: Liquid flow rate
u_{melt}	: Average melt flow velocity
t	: Average melt depth
V	: Cutting speed
W	: Average kerf width
ρ	: Material density

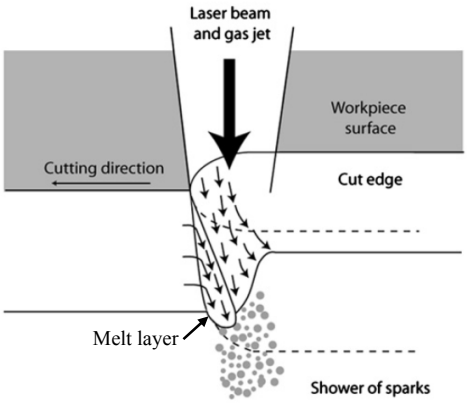

Fig. 1. The laser cutting process (Powell 2011).

During the process a thin layer of melt flows down the cut front, as shown in Fig. 1. Tani (2004) explains that the creation of both dross at the bottom of the kerf and striations on the cut edge (surface roughness) depend on the melt film condition throughout the kerf.

Schulz (1999) explains that dross formation is related to properties of the melt such as its thickness and velocity. He compared this to the experimental observations of viscous free surface flows around an edge, and the separation of the flow from the solid.

The importance of the melt film on the cut front is also emphasized by Chen (1999) who concludes that fluctuations in the absorbed laser power and the velocity of the high speed gas jet can create perturbations in the melt film which in turn could give rise to fluctuating striation patterns on the cut edge. It is therefore clear that information about the melt film thickness and velocity could give more insight into quality parameters in laser cutting.

Laser cutting of steels can be divided into two main subjects i.e. laser fusion cutting of stainless steel (usually with nitrogen assist gas) and laser oxygen cutting of mild steel with oxygen gas assist.

In both cases the assist gas is used as a source of mechanical energy to blow away the melt in the kerf. In laser oxygen cutting the oxygen assist gas also functions as a source of heat since the oxygen undergoes an exothermic reaction with the iron in meld steel. However, the gas pressures used in the two techniques are markedly different. Oxygen pressures tend to be less than 2 bar and nitrogen pressures are usually in excess of 10 bar. For this reason the melt film behavior for laser oxygen cutting and laser fusion cutting are separately discussed in section 1.1 and 1.2 respectively.

1.1. Melt film behavior in laser oxygen cutting

The melt velocity and melt thickness were measured by Dubrov (2011) with the use of two spectrometers to measure the temperature along the cut front. He estimated a melt speed of 8m/s and reported that this speed coincided with the velocity of the local temperature minimum along the cut front. From this the melt thickness was estimated to be 20μm. The presence of capillary waves which introduced noise into the temperature measurements was also discussed. These capillary waves had wavelengths ranging from 5-300μm. Waves with 24μm wavelength had a phase velocity of 8m/s which is equal to the temperature based melt velocity measurement.

Chen (1999, 2001) reported the existence of a thin melt that becomes unstable and generates slow waves at the melt surface. Chen further calculated the surface velocity with a model based on linearized two-dimensional Navier-Strokes equations. The melt speeds were found to have values between 0.4-0.7m/s and melt thickness was between 16-26μm for cutting speeds between 10-70 mm/s (0.6 – 4.2m/min).

Wee & Li (2005) solved mass, momentum and power equations to obtain the melt thickness for laser oxygen cutting of mild steel. They calculated a maximum melt thickness of approximately 75μm with corresponding maximum surface velocity of 2.5m/s for a 3mm plate.

Yilbas (2006) predicted the dross diameter for 1.5mm mild steel processed with a 2kW CO2 pulsed laser oxygen cutting by the use of lump parameter analysis (a simplification of a physical system under certain assumptions). In order to determine the dross formation he modeled the liquid layer on the melt front. For a cutting gas velocity of 50m/s he obtained a melt velocity of 1.5m/s and melt thickness of 165μm. Increasing the gas velocity to 150m/s increased the melt velocity to 4.5m/s with a melt thickness of 60μm. As expected the melt thickness decreases due to the increased shearing force of the gas jet. Yilbas validated his model only for the dross diameter and not for the melt thickness.

Others such as Tani (2003) and Kaplan (1996) have created analytical models of the melt film geometry (inclination angle, melt film thickness) and melt film velocity. Tani obtained a maximum melt speed of 3m/s for simulations considering a 2kW CO2 laser source, while Kaplan obtained a melt thickness of 70μm at 0.5bar oxygen pressure for a 6mm mild steel plate and CO2 laser cutting.

1.2. Melt film behavior in laser fusion cutting

Wandera (2010) modeled the melt film velocity and corresponding melt thickness and compared this with an experimentally determined position at which the flow inside the cut front becomes turbulent (the so called boundary layer point) for 10mm stainless steel with a cutting speed of 1m/min and 5kW fiber laser. She suggested a melt velocity between 1400-2200 m/s with a melt thicknesses of 0.2-0.4μm for a nitrogen gas pressure between 16-18bar and kerf width between 600-800μm. These values are unrealistic as they would imply a process which would be entirely dominated by evaporation rather than the actual process which involves the ejection of molten particles several tens of microns in diameter.

Hirano (2011) investigated the hydrodynamics of the melt layer in laser cutting of low carbon mild steel with nitrogen assist gas by using a high speed imaging camera. He found a melt velocity of 3.2m/s while the velocity of the so called observed humps was 0.2m/s. He explains that the difference in velocity is due to the fact that the evolution of the hump is not due to a mass flow but due to a phase evolution. Both Golubdev (2003) and Hirano (2011) describe humps as melt accumulations which rest on top of so called shelves. These shelves have been shown to slide down along the cut front by Hirano. However, Hirano performed his experiments with parameters which are very different from the ones used in actual laser cutting. He used a focus spot diameter of 1.7mm (industry standard 0.2 – 1.0 mm) and a cutting gas pressure of 2.5bar (industry standard 10 – 16bar).

Ermolaev (2014) filmed the cut front from the side via a transparent plate with a high speed camera. He studied melt flow, melt removal and striation formation. He found that for CO2 laser cutting there exists a well-developed coherent stream of liquid, while for fiber laser cutting the melt flow is highly unstable with multiple melt ejections from the cut front to the side walls.

Kaplan (1996) obtained a melt thickness of 20μm and melt velocity of 7m/s for a 3mm mild steel plate and CO2 laser cutting with nitrogen assist gas.

In this paper HSI techniques are used to investigate the flow conditions within the cut zone. Of particular interest are: melt flow velocity, melt thickness and cut front morphology. These results are unique in the published literature because they use normal cutting conditions. Previous experimental work has used exaggerated cut widths and unrealistic cutting gas pressures.

2. Material and methods

The observation of melt flow down a laser induced cutting front is experimentally rather difficult because the cut front is narrow and surrounded by the recently cut walls of the kerf. For this reason most studies of the cut front involve cuts started at the edge of the sheet – where the cut front is most visible. However, this approach can give misleading results because the cut front is, at this point, in its 'start up' phase rather than its eventual quasi steady state.

To overcome this problem a new experimental technique was developed which allows the high speed imaging (HSI) camera a view of the well-established quasi steady state cut front. This involves using the laser to produce a cut path which results in the sudden falling away of a triangular cut part to expose the cutting front in action.

The cutting path used is explained in Fig. 2. First the laser cuts along line 1, then returns to the edge of the material and cuts to the intersection along line 2 (without stopping at the intersection). As the laser reaches the intersection the triangle enclosed by lines 1 and 2 and the edge of the material falls away – revealing the steady state cut front as it continues to cut line 2.

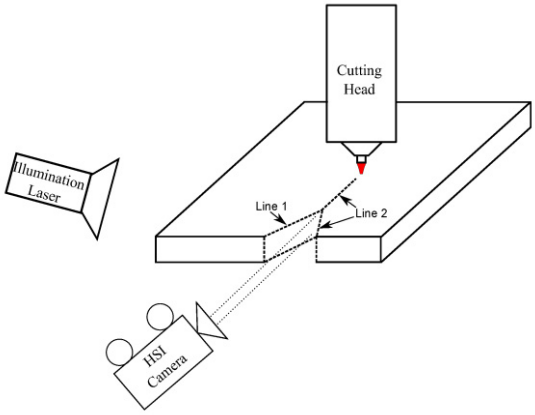

Fig. 2. HSI Experimental setup.

Table 1 shows the cutting parameters and Table 2 shows the laser beam parameters used in this experiment. The material used was 10mm stainless steel AISI 304 (EN 1.4301). The laser used was a Bystronic BySprint Fiber 3015 with a Fiber 6000 resonator.

Table 1. Cutting parameters used.

Parameters	Values
Thickness	10mm
Cutting speed	1.8m/min
Laser power	6000W
Focal position	-12mm
Gas type & pressure	N_2 & 16bar
Nozzle diameter & type	3.5mm (Bystronic HK35)
Nozzle standoff distance	0.8mm

Table 2. Laser beam parameters.

Parameters	Values
Fiber diameter	100μm
Focusing lens focus distance	200mm
Collimation lens collimation distance	100mm
Beam focus diameter	200μm

A Redlake NR4-S2 high speed camera was used with following setup parameters:

- Frame rate of 4000 frames per second with spatial resolution of 512 x 496 pixels
- 105mm Micro-Nikkor lens with focal ratio f/4
- Band pass filter which blocks process light & matches the illumination wavelength, as described by Frostevarg (2014)
- Illumination Laser: Cavilux HF diode illumination Laser with 810nm wavelength

Particle tracking velocimetry (PTV) was employed to measure the velocity of bright patches on the melt surface as they flow towards the bottom of the kerf. PTV determines the velocity of individual particles in flows and is based on the Lagrangian reference frame. The Lagrangian reference frame observes fluid motion by tracking an individual feature as it moves through space and time. The algorithm first isolates individual features on the cut front in each frame of the high speed video. In order to find valid correspondences between features in different frames the temporal matching problem was solved with cross-correlation algorithms, relaxation algorithms or a combination of both as described in Brevis (2010).

3. Results and discussion

Fig. 3 shows a schematic of the set up for high speed imaging and makes two important points:

1. The melt surface is not flat
2. The melt flow rate is faster towards the melt surface and slower towards the melt/solid interface.

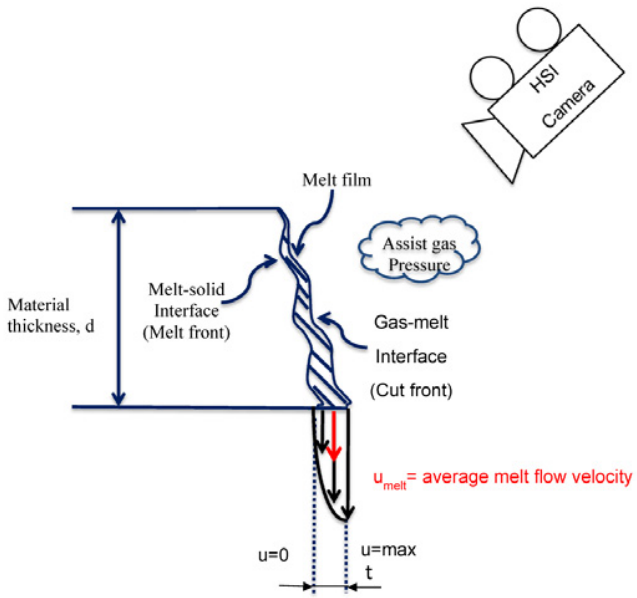

Fig. 3. The High Speed Imaging set-up.

Fig. 4 shows diagrammatically that there are two entirely independent ways of working out the mass flow rate out of the cut zone. The first of these can be called the kerf removal rate and is simply calculated from the kerf width, the material thickness and the cutting speed, as in Equation (1):

$$Kr = W \cdot d \cdot V \cdot \rho \tag{1}$$

Where:	Kr:	Kerf removal rate	(g/s)
	W:	Average kerf width	(mm)
	d:	Material thickness	(mm)
	V:	Cutting speed	(mm/s)
	ρ:	Material density	(g/mm^3)

Equation 1 is only valid for cutting speeds (V) that enable sufficient heat input into the material for cutting to occur.

The second method of working out the mass flow rate involves working out the liquid flow rate out of the bottom of the kerf. For this the fluid stream cross section ((π/2) x kerf width x average melt depth) and the average melt flow speed of the stream (u_{melt}) is needed.

$$Lr = \frac{\pi}{2} \cdot W \cdot t \cdot u_{melt} \cdot \rho \tag{2}$$

Where:	Lr:	Liquid flow rate	(g/s)
	t:	Average melt depth	(mm)
	u_{melt}:	Average melt flow velocity	(mm/s)

As a mass balance it is assumed that Kr = Lr with W, d, V and ρ directly measurable. With this information the flow characteristics in the cut zone can then be investigated. Pocorni (2014) explains that the maximum temperature in the cut zone is proportional to cutting speed. As the current work does not include cutting of thin section material at very high speeds, mass loss as a result of vaporization is minimal and is left out of the mass balance.

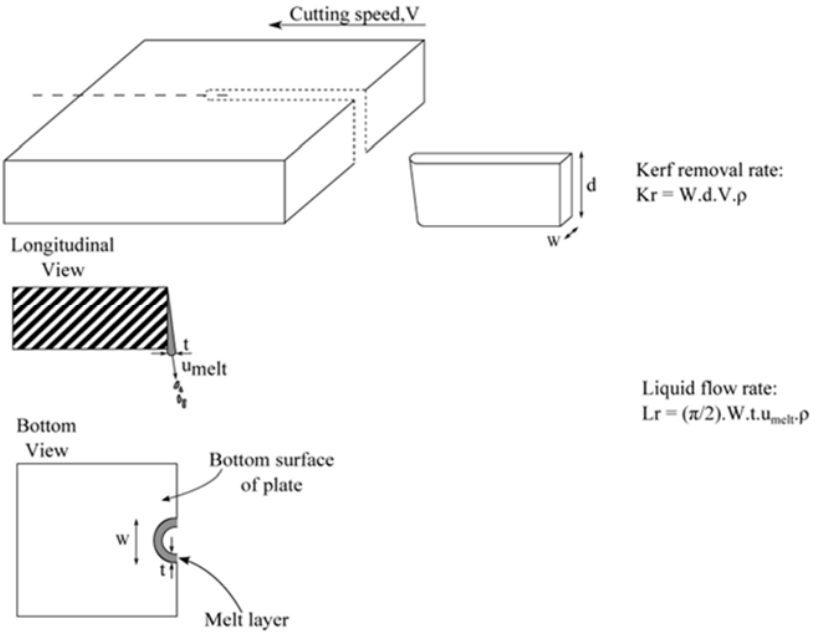

Fig. 4. Two different ways of working out the mass flow rate out of the cut zone.

Measuring the flow rate of the liquid stream is experimentally difficult because the kerf is very narrow and there are no markers to follow the flow on the liquid surface. HSI was used to measure the downward velocity of bright spots on the liquid surface (see Fig. 5) and this gave the results shown in Fig. 6 (a).

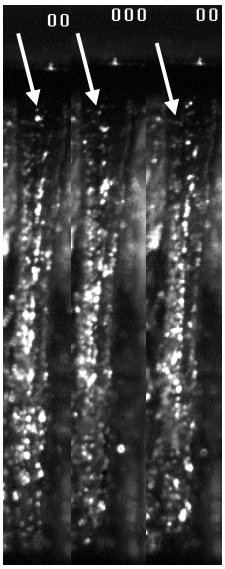

Fig. 5. Three frames from the HSI film showing the movement of a bright spot down the cut front. The frame rate was set to 4000 frames per second thus giving a time difference of 0.25ms between frames.

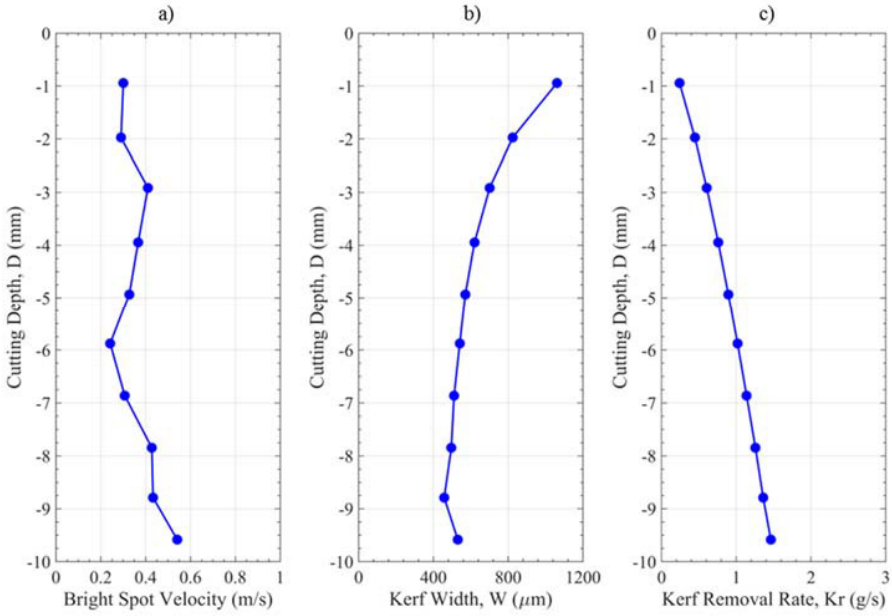

Fig. 6 (a) Bright spot velocity; (b) Kerf width; (c) Kerf removal rate.

Fig. 6 (b) gives the kerf width as a function of cutting depth and from this and the cutting speed it is possible to calculate the kerf removal rate (Kr) as a function of cutting depth (Fig. 6 (c)). As a first approximation the simplified melt geometry shown in Fig. 4 is assumed. Given this geometry and the kerf removal rate (Fig. 6 (c)), the flow

velocities given by the HSI measurements (Fig. 6 (a)) would require a melt thickness (t) of approximately 1mm in the bottom half of the kerf, which is not compatible with an average kerf width of 0.6mm.

Clearly then, the bright spot velocities given in Fig. 6 (a) are related to a feature of the flow which is not the surface flow velocity. It seems probable then that the bright spots in the HSI video correlate with humps below the melt surface which are eroded by a combination of hot fluid flow and enhanced laser beam absorption, so that they move down the cut front. Fig. 7 presents a schematic cross-sectional view of this type of cut front.

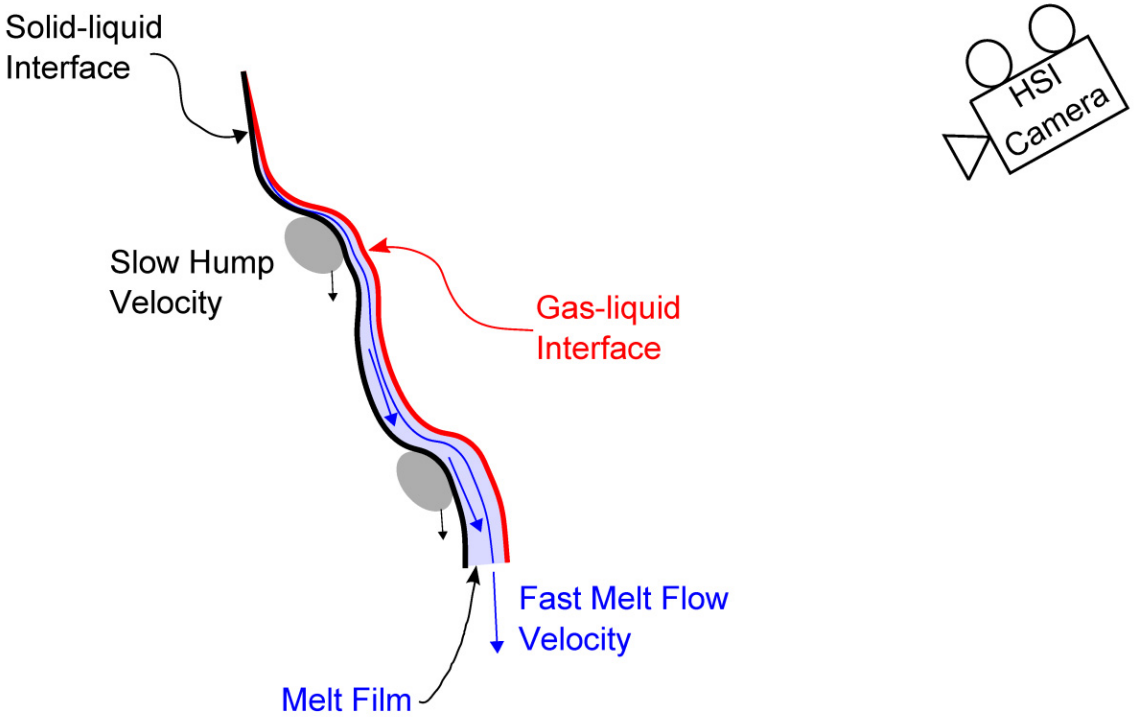

Fig. 7. The morphology of the cut front (longitudinal cross section).

The existence of moving bumps is supported by SEM images and cross sections of the solidified cut front as shown in Fig. 8 (a). Fig. 8 (b) shows the bumps more clearly because the image has been expanded in the x direction.

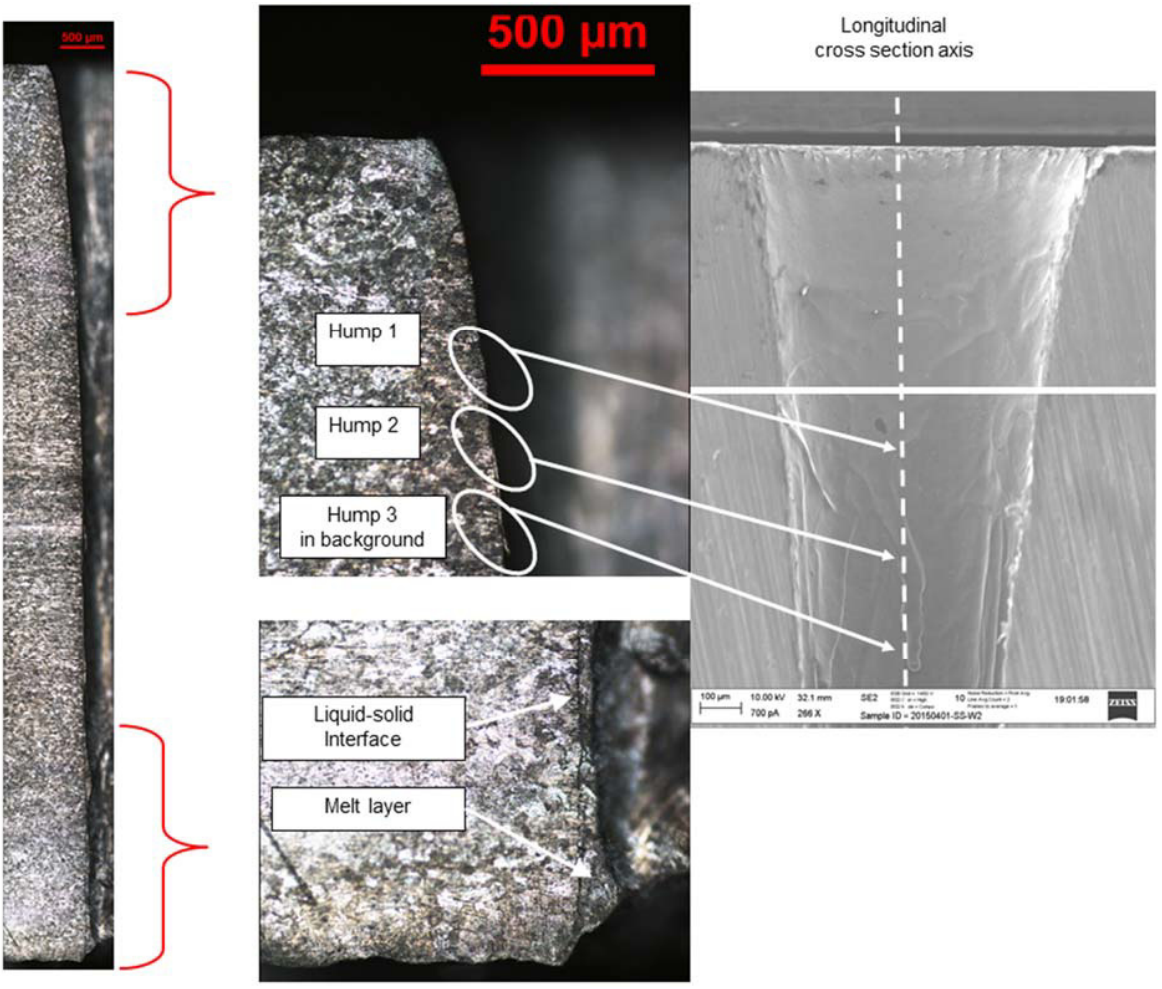

Fig. 8 (a) Longitudinal cross sections of the solidified cut front with SEM image of the cut front face

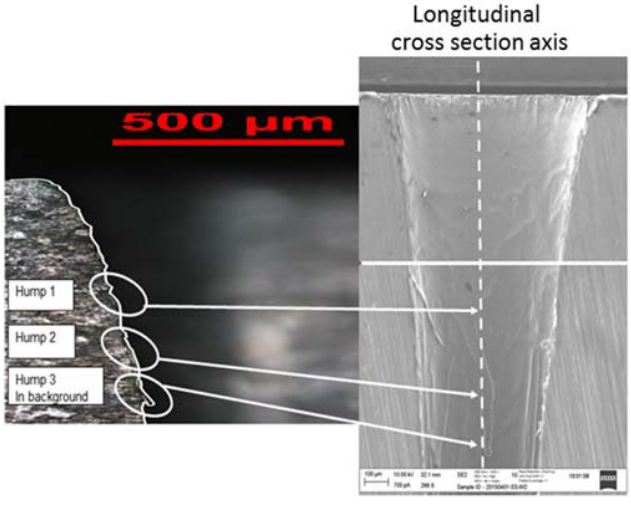

Fig. 8 (b) Longitudinal cross section of the cut front – Image expanded in the x direction to show the bumps more clearly.

As HSI cannot be used to directly measure the flow rate of the liquid down the cut front an HSI video was taken of the droplets being ejected from the bottom of the cut zone. Although these droplets are accelerated by the gas jet and by gravity, their velocity during their first millimetre of flight will reflect the speed of the liquid flow they were ejected from. In-flight speed measurements of these droplets are presented in Fig. 9. The average flow rate was 1.1m/s with a velocity range between 0.5 and 2.2m/s. This range is probably due to the range of flow rates in the liquid stream on the cut front (low flow rates at the liquid-solid interface, maximum flow rates on the outer surface of the melt). As a first approximation an average melt flow velocity of 1.1m/s at a cutting speed of 1.8m/min and kerf width of approximately 0.5mm gives a melt depth at the bottom of the kerf of approximately 0.17mm, which is not unreasonable.

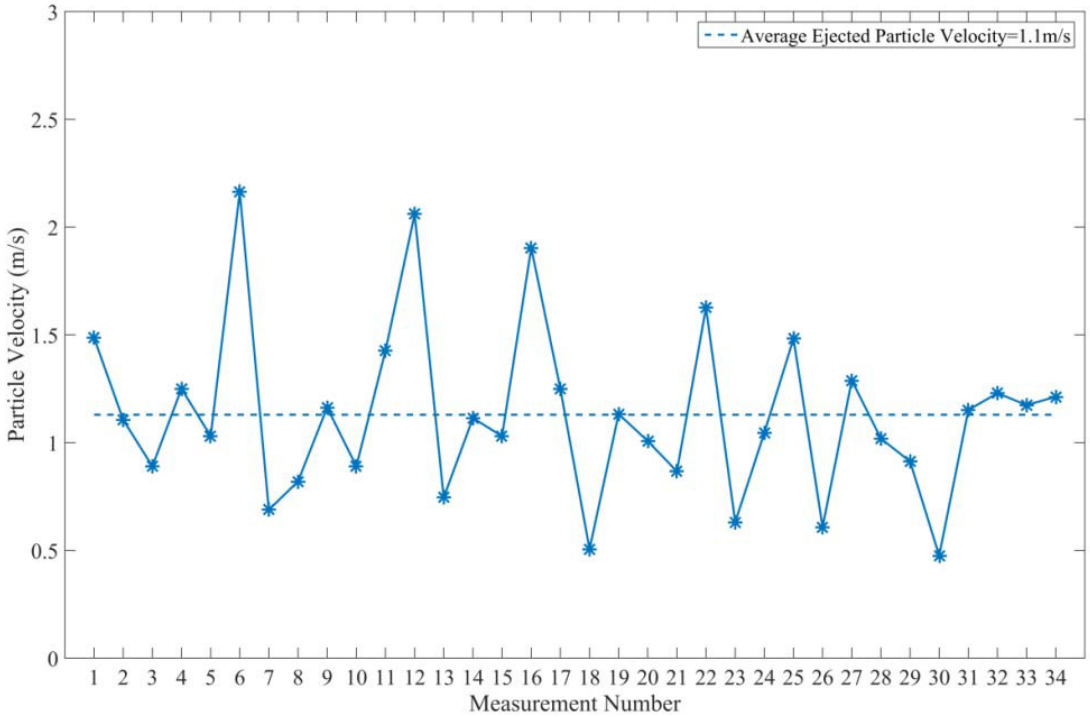

Fig. 9. The velocity of a number of droplets in the first 1mm of their flight out of the bottom of the kerf.

4. Conclusions

The results presented here suggest that the cut front produced when cutting stainless steel with a fibre laser and a nitrogen assist gas is covered in bumps which themselves are covered in a thin layer of liquid. Under the conditions shown here the bumps move down the cut front at an average speed of approximately 0.4m/s. The liquid flows at an average speed of approximately 1.1m/s. The average melt depth at the bottom of the cut zone is approximately 0.17mm. These results depended on a new experimental technique which allowed HSI observation of cuts carried out under standard cutting parameters.

Acknowledgements

The support of this work by the European Commission through the Seventh Framework Programme (FP7) within the HALO project (Grant Agreement Number 314410) is gratefully acknowledged.

References

Brevis, W., Niño, Y., & Jirka, G. H. 2010. Integrating cross-correlation and relaxation algorithms for particle tracking velocimetry. Experiments in Fluids 50, 135–147.

Chen, K., & Yao, Y. L. 1999. Striation formation and melt removal in the laser cutting process. Journal of Manufacturing Processes 1, 43–53.

Chen, K., Yao, Y. L., Modi, V., Engineering, M., & York, N. 2001. Gas Dynamic Effects on Laser Cut Quality. Journal of Manufacturing Processes 3, 38–49.

Dubrov, A. V., Dubrov, V. D., Zavalov, Y. N., & Panchenko, V. Y. 2011. Application of optical pyrometry for on-line monitoring in laser-cutting technologies. Applied Physics B: Lasers and Optics 105, 537–543.

Ermolaev, G. V, Yudin, P. V, Briand, F., Zaitsev, A. V, Kovalev, O. B., & Briand, F. 2014. Fundamental study of CO2- and fiber laser cutting of steel plates with high speed visualization technique. Journal of Laser Applications 26.

Frostevarg, J. (2014). PhD Thesis: The Morphology of Laser Arc Hybrid Welds.

Golubev, V. S. 2003. Problems of Hydrodynamics in the Processes of Laser Welding and Cutting. In: B. E. Paton & V. S. Kovalenko (Ed.). Laser Technologies in Welding and Materials Processing, Katsiveli, Crimea, Ukraine, Electric Welding Institute, NASU, pp. 24–31.

Hirano, K., & Fabbro, R. 2011. Experimental investigation of hydrodynamics of melt layer during laser cutting of steel. Journal of Physics D: Applied Physics 44, 105502.

Kaplan, A. F. H. 1996. An analytical model of metal cutting with a laser beam. Journal of Applied Physics 79, 2198–2208.

Pocorni, J., Petring, D., Powell, J., Deichsel, E., & Kaplan, A., 2014. Differences in Cutting Efficiency between CO2 and Fiber Lasers when Cutting Mild and Stainless Steels, 33rd International Congress on Applications of Lasers and Electro-Optics (ICALEO), San Diego, USA, paper #905

Powell, J., Al-Mashikhi, S. O., Kaplan, A. F. H., & Voisey, K. T. 2011. Fibre laser cutting of thin section mild steel: An explanation of the 'striation free' effect. Optics and Lasers in Engineering 49, 1069–1075.

Schulz, W., Kostrykin, V., Nießen, M., Michel, J., Petring, D., Kreutz, E. W., & Poprawe, R. 1999. Dynamics of ripple formation and melt flow in laser beam cutting. Journal of Physics D: Applied Physics 32, 1219–1228.

Tani, G., Tomesani, L., & Campana, G. 2003. Prediction of melt geometry in laser cutting. Applied Surface Science 208-209, 142–147.

Tani, G., Tomesani, L., Campana, G., & Fortunato, A. 2004. Quality factors assessed by analytical modelling in laser cutting. Thin Solid Films 453-454, 486–491.

Wandera, C., & Kujanpaa, V. 2010. Characterization of the melt removal rate in laser cutting of thick-section stainless steel. Journal of Laser Applications 22, 62.

Wee, L. M., & Li, L. 2005. An analytical model for striation formation in laser cutting. Applied Surface Science 247, 277–284.

Yilbas, B. S., & Aleem, B. J. A. 2006. Dross formation during laser cutting process. Journal of Physics D: Applied Physics 39, 1451–1461.